Journal of Sound and Vibration 329 (2010) 5532–5545

Contents lists available at ScienceDirect

Journal of Sound and Vibration

journal homepage: www.elsevier.com/locate/jsvi

Vibro-acoustic radiation of rigid bodies oscillating at large amplitude and low Mach number: Modelling and experiments

N. Bert Roozen [a,b,*], Tim Rutjes [b,1], Henk Nijmeijer [a]

[a] Section Dynamics and Control, Department of Mechanical Engineering, Eindhoven University of Technology, P.O. Box 513, 5600 MD Eindhoven, The Netherlands
[b] Philips Applied Technologies, High Tech Campus 7, 5656AE Eindhoven, The Netherlands

ARTICLE INFO

Article history:
Received 27 July 2009
Received in revised form
5 July 2010
Accepted 6 July 2010
Handling Editor: L. Huang
Available online 21 August 2010

ABSTRACT

The acoustic radiation of vibrating bodies can usually be considered as a linear phenomenon as in most cases the vibration amplitudes of oscillating bodies are small compared to their dimension. However, in case of large amplitude and small Mach number, the large displacement amplitude of a vibrating body gives rise to geometric nonlinear acoustic effects. In this paper it is shown that the nonlinearity causes an asymmetry in the time signal of the radiated pressure as observed at a fixed position, resulting in harmonic distortion of the radiated sound field. These nonlinear effects can be analysed by the finite element method, using a linear fluid behaviour in combination with a moving mesh approach. This approach is implemented and used to predict the nonlinear sound radiation of lithographic stages oscillating at large amplitude and low Mach number. Acoustic experiments prove the validity of the analysis technique for the geometrical nonlinear phenomena. In addition the structural response of a nearby body excited by the nonlinear acoustic radiation of the stage is calculated and verified experimentally.

1. Introduction

Harmonic distortion of acoustic waves due to geometric nonlinearities can be encountered in acoustic radiation from bodies moving with large amplitudes. In recent measurements in a lithographic wafer stepper harmonic distortion caused significant acoustic responses at frequencies that were not present in the frequency content of the exciting stage movement. The recognition of harmonic distortion due to geometric nonlinearities is important for high precision machines. In the sub-nano accuracy range of the present and future lithographic scanners acoustic disturbances will play a significant role. The acoustic sound field radiated by the oscillating stages can set parts of the lithographic machine into vibration, with disastrous effects on machine performance (see Fig. 1).

One approach which is followed by industry is the use of accurate and effective (feed-forward) control loops to minimize the (acoustic) disturbances due to stage movements. If the harmonic distortions are not included in the model that governs the control loop, the feed-forward control loop will not be able to compensate for it, and this may seriously affect the overall control design. Building the model for the control loop requires a good understanding of all relevant phenomena. Finite element (FE) modelling of large amplitude vibrations is very useful for understanding the harmonic distortion, and studying the influencing parameters. A reduced model, based on FE, measurements or empirical methods, can be used to create the model for the (feed-forward) control loop.

* Corresponding author at: Section Dynamics and Control, Department of Mechanical Engineering, Eindhoven University of Technology, P.O. Box 513, 5600 MD Eindhoven, The Netherlands.
E-mail address: n.b.roozen@tue.nl (N. Bert Roozen).
[1] Present address: Peutz B.V., P.O. Box 66, 6585 ZH Mook, The Netherlands

0022-460X/$ - see front matter © 2010 Elsevier Ltd. All rights reserved.
doi:10.1016/j.jsv.2010.07.002

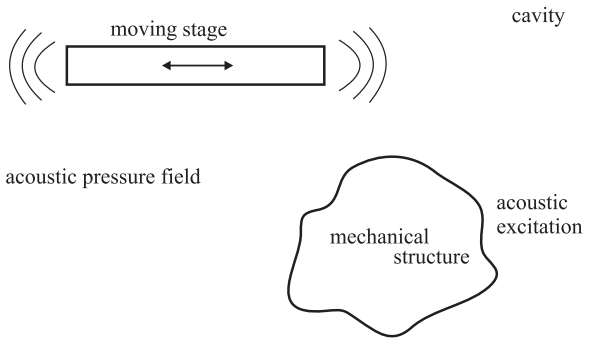

Fig. 1. Generalization of the acoustic excitation problem for lithographic machines; a moving stage that acoustically excites parts of a mechanical structure in some cavity.

In literature the sound waves generated by the motion of a solid body are usually considered using linear theory [1]. This is justified as in most cases the vibration levels are much smaller than the typical dimension of the vibrating body. However, large amplitude vibration, in the absence of fluid nonlinearities, is a source of harmonic distortion. Little literature is available on this topic. Only one paper, written in 1975 by Frost [2], illustrates the phenomenon for a harmonically pulsating and a harmonically oscillating rigid sphere. The work of Frost et al. found its applications in the study of oscillating gas bubbles as sources of sound in liquids [3,4]. When the amplitude of oscillation (and the Mach number) is small, the sound pressures are associated only with the volume pulsation, and occur at the pulsation frequency. However, when the amplitude of the oscillation is large as compared to the overall dimension whilst the Mach number is still small, acoustic energy is radiated at the pulsation frequency and its harmonics. This nonlinear effect is not caused by nonlinearities in the medium. It is caused by the large displacement of the radiating structure [2]. This physical characteristic implies that this phenomenon can be analysed by the finite element (FE) method, using a linear constitutive model for the acoustic medium, and a mesh adaptation to describe the large displacements.

In this paper emphasis is placed upon the physical understanding of the geometric nonlinear effects with a moving stage of a wafer stepper as application. To allow for an accurate prediction of the sound pressures radiated by an oscillating stage at large displacement amplitudes, a FE model has been set up including the geometric nonlinear effects. The FE model has been verified by means of dedicated experiments. In these experiments the response of a polystyrene ball hanging in close proximity to the moving stage, being excited by the acoustic waves radiated by the stage, has been measured. The aim of this experiment is to demonstrate the validity of the FE model to predict both the nonlinear acoustic pressure field and the subsequent acoustic excitation of nearby secondary structures. The ball represents a solid body such as the lens of a lithographic apparatus, which is brought into vibration by the acoustic waves radiated by the stage. A ball is chosen, instead of lithographic solid bodies such as the lens, for a number of reasons. At low frequencies (say below a few hundred Hz) the lens of a lithographic apparatus behaves as a rigid body, its internal resonance frequencies lying well beyond this frequency range. A rigid ball would suffice from this perspective. Another reason is to prevent modelling difficulties due to complex geometries. A ball is well defined in terms of geometry and in terms of structural dynamics in the frequency range considered. Finally, for a given pressure disturbance acting on the ball, the rigid body vibration levels of the ball scale linearly with the reciprocal value of its mass. For this reason the vibration levels of the ball were higher and possible measurement problems were prevented. Note that the lens of a lithographic apparatus nowadays may not vibrate more than a few nanometres to prevent, for instance, overlay issues on the wafer.

Using this configuration the geometric nonlinear effect is studied in detail, both experimentally and numerically. An arbitrary Lagrangian–Eulerian (ALE) formulation is used in the numerical model to tackle the geometric nonlinear effects, by means of an adapting moving mesh.

This paper is organized as follows. In Section 2, the description of the nonlinear FE-model is given. The approach to describe the fluid with a linear material model and to take the geometric nonlinearity into account by means of a moving FE mesh, is treated in this section. Numerical simulations of a stage moving at high displacements, acoustically exciting a secondary structure in its neighbourhood are discussed. Based upon the simulation results the physical aspects related to the nonlinear phenomenon that are responsible for the harmonic distortion are treated. In Section 3, the verification experiments are discussed. It is shown that frequency components that are not present in the set-point of the stage movements do appear in the acoustic sound fields and in the response of the spherical rigid body due to the nonlinear effects. The finite element implementation is validated by these experiments. Finally in Section 4, conclusions are drawn.

2. Model description

This section presents a three dimensional FE-model that describes the acoustic radiation of structures oscillating at large displacement amplitudes. The large amplitudes cause a geometric nonlinear effect that results in harmonic distortion in the fluid, although the fluid still behaves linearly. The 3-D FE model takes into account the geometric nonlinear effects by means of

an arbitrary Lagrangian–Eulerian (ALE) formulation, resulting in harmonic distortion of the radiated acoustic field. It also offers the possibility to calculate the structural-acoustic response of a (flexible) structure being excited by the radiated acoustic field.

The applicability of the models developed in this paper is primarily dependent on the acoustic Mach number. The acoustic Mach number M at the surface of the oscillator is given by [5]

$$M = \frac{v_{\max}}{c}, \tag{1}$$

where $v_{\max}$ is the maximum velocity of the radiating oscillator surface and c is the speed of sound. In this paper, it is assumed that the Mach number is much smaller than unity, which implies that fluid nonlinearities can be neglected.

Our concern, however, is with the oscillation of rigid bodies whose displacement amplitude is of the order of their characteristic dimension, i.e. for which

$$\left(\frac{u_{\max}}{a}\right) = \mathcal{O}(1), \tag{2}$$

where $u_{\max}$ is the maximum displacement amplitude of the radiating oscillator surface and a is a typical dimension of the rigid body. Rewriting the Mach number as

$$M = \frac{u_{\max}\omega}{c} = u_{\max}k = \left(\frac{u_{\max}}{a}\right)ka, \tag{3}$$

where ω is the angular frequency and k is the acoustic wavenumber, it can be seen from Eq. (2) and the requirement that the Mach number should be small, that ka should be small:

$$ka \ll 1. \tag{4}$$

In practice, this means that the assumptions only hold for bodies oscillating at low frequencies. In case of the aforementioned stage for lithographic machines, with a typical dimension of 0.1 m (the height of the stage) and an oscillating frequency of 3.5 Hz, operating in air, the requirement given in Eq. (4) is satisfied.

2.1. Nonlinear finite element based model description

A numerical, discrete FE model has been set up in COMSOL Multiphysics ® (Comsol, Los Angeles, CA), a multiphysics FE tool. The problem being considered is that of a rigid body moving in a volume filled with air. The moving rigid body generates acoustic sound fields, which in turn excite secondary mechanical structures in the neighbourhood of the moving body as illustrated in Fig. 1. Thus, we have two structural domains and one acoustic domain, which constitutes a true, fully coupled multiphysics problem. In the next subsections each sub domain will be discussed, including its boundary conditions and its coupling conditions. The geometric nonlinearity is taken into account by means of a remeshing technique, which will be described as well.

2.1.1. Acoustic domain

The acoustic domain comprises the volume of air around the moving body and the secondary structure (i.e. the ball). The air has a density of $\rho_0 = 1.25\,\mathrm{kg\,m^{-3}}$ and a speed of sound $c = 344\,\mathrm{m\,s^{-1}}$. The pressure, $p(x,y,z)$, is calculated using the time harmonic formulation based on the homogeneous Helmholtz equation:

$$\nabla \cdot \left(-\frac{1}{\rho_0}\nabla p\right) - \frac{\omega^2 p}{\rho_0 c^2} = 0. \tag{5}$$

2.1.2. Structural domains

The secondary structure (i.e. the ball), which is brought into motion by the radiated acoustic fields, is modelled as a rigid body. The equation that is used to calculate the global displacements of the secondary structure is

$$m\frac{\partial^2 \mathbf{u}}{\partial t^2} = \mathbf{F}, \tag{6}$$

where m is the mass of the rigid body, $\mathbf{u} = (u,v,w)'$ are the global displacements in the x-, y- and z-directions, and where $\mathbf{F}$ is the integrated force over the surface A of the secondary structure, due to the coupling with the acoustic domain:

$$\mathbf{F} = \int_A \mathbf{F}_n \,\mathrm{d}A. \tag{7}$$

The force per unit area $\mathbf{F}_n$ ($\mathrm{N\,m^{-2}}$) is described below.

2.1.3. Coupling

The acoustic and structural domains are fully coupled. The coupling of the acoustic field to the secondary structure is modelled by specifying an edge load on the boundaries of the secondary structure. As the pressure, p, works in normal direction to the boundaries of the secondary structure, only a normal force component per unit area $\mathbf{F}_n$ ($\mathrm{N\,m^{-2}}$) exists, given by

$$\mathbf{F}_n = p \cdot \mathbf{n}, \tag{8}$$

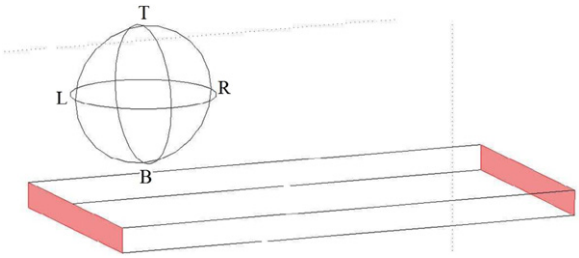

Fig. 2. Structural domain model and stage boundary conditions (grey surfaces). The letters L,R,T,B indicating the positions relative to the ball.

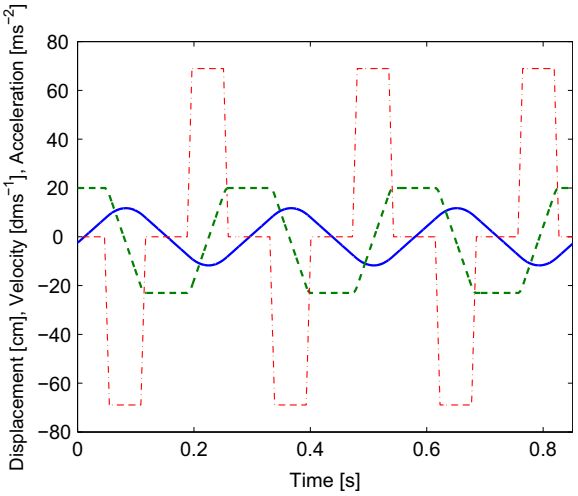

Fig. 3. Set-point of the stage movement, ——— displacement, - - - - - - - - velocity, — · — · — · — · — · acceleration.

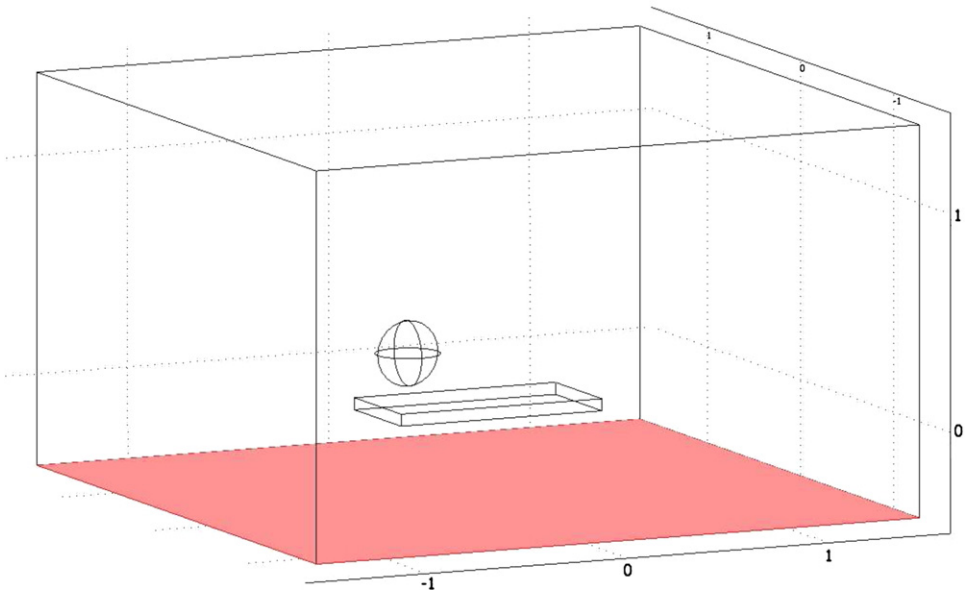

Fig. 4. Idealization of acoustic cavity with reflecting floor (grey surface), stage and ball.

where $\mathbf{n}$ is the surface normal. The coupling of the vibrating secondary structure to the acoustic domain is taken into account by equating the acoustic particle accelerance $\mathbf{n}\cdot\nabla p/\rho_0$ to the structural accelerance of the secondary structure a_n,

$$\mathbf{n}\cdot\nabla p/\rho_0 = a_n. \tag{9}$$

2.1.4. Structural domain geometry and boundary conditions

The geometry of the structural domain is given in Fig. 2, comprising a rigid ball and a rigid stage. The stage is modelled as a rectangular shoe box, with dimensions $1\times0.5\times0.055$ m, moving from left to right in the direction of the longest dimension. The ball is modelled as a sphere with a radius of 0.15 m. The clearance between the ball and the moving stage is 0.08 m.

To prevent the ball from drifting away a very weak spring is modelled. The three dimensional spring is modelled in x-, y-, and z-directions by specifying a body force per unit area, $\mathbf{F}_s$ ($\mathrm{N\,m^{-2}}$)

$$\mathbf{F}_s = \frac{-s\mathbf{u}}{A}, \tag{10}$$

where s is the spring stiffness and A is the surface area of the secondary structure. A spring stiffness $s=1.2\,\mathrm{N\,m^{-1}}$ is used. This choice is based upon the experimental observation of a pendulum frequency of 0.343 Hz (see Section 3.3). Suspending

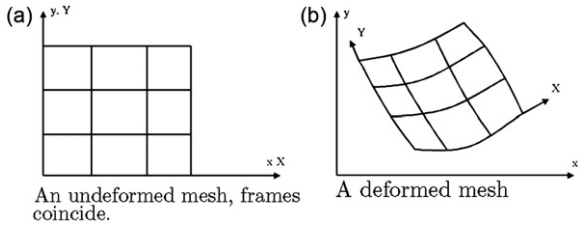

Fig. 5. Example of mesh with spatial frame (x,y) and reference frame (X,Y).

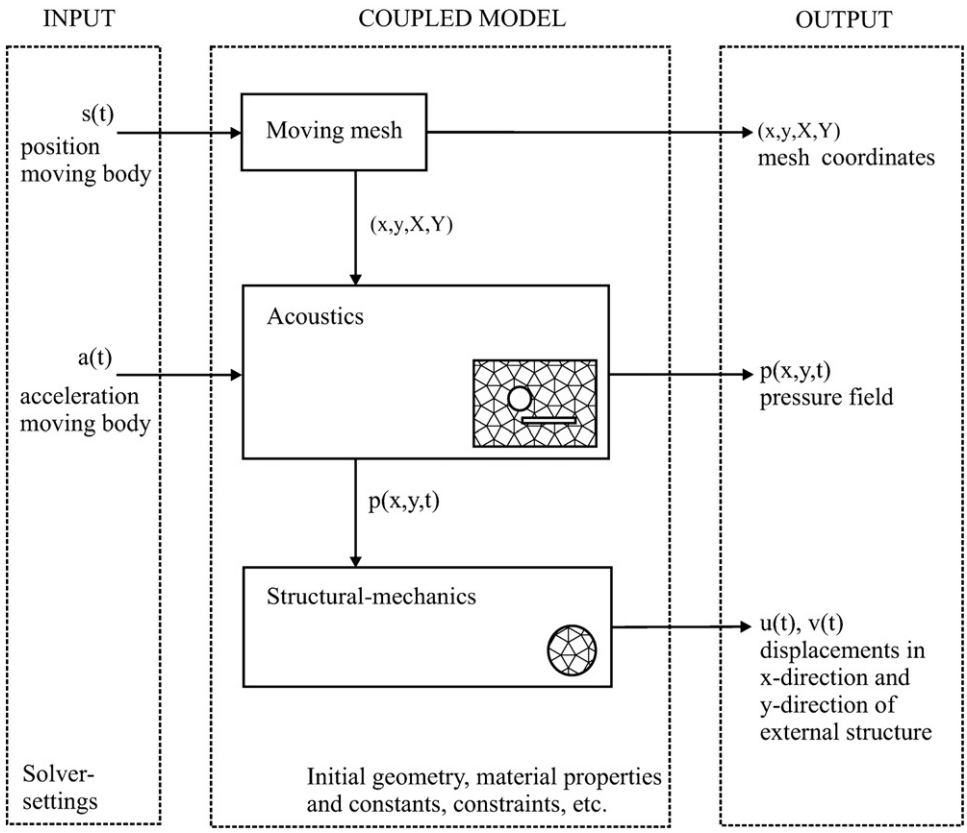

Fig. 6. Comsol multiphysics coupling.

the ball weighting 0.2674 kg with a spring of given stiffness, results in an eigenfrequency of 0.343 Hz, which represents the pendulum behaviour of the ball hanging on a wire.

2.1.5. Acoustic domain geometries and boundary conditions

The movement of the stage is modelled as a prescribed acceleration, which is specified as an acoustic boundary condition on the moving edges. At the left and right boundary of the moving body, as illustrated by the grey surfaces

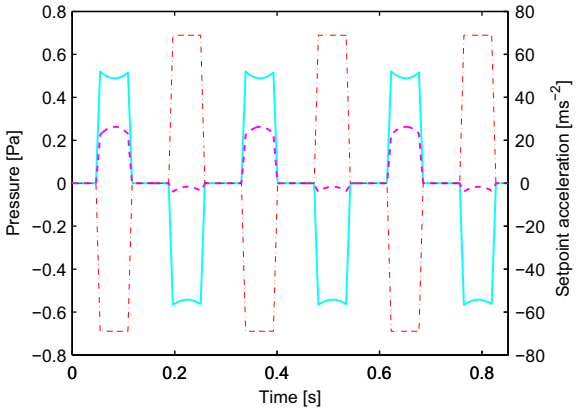

Fig. 7. Numerically predicted sound pressure close to the ball due to stage movements, ——— pressure p_L, - - - - - - - - pressure p_R, – · – · – · – · – · setpoint acceleration. See Fig. 2 for the locations L and R close to the ball.

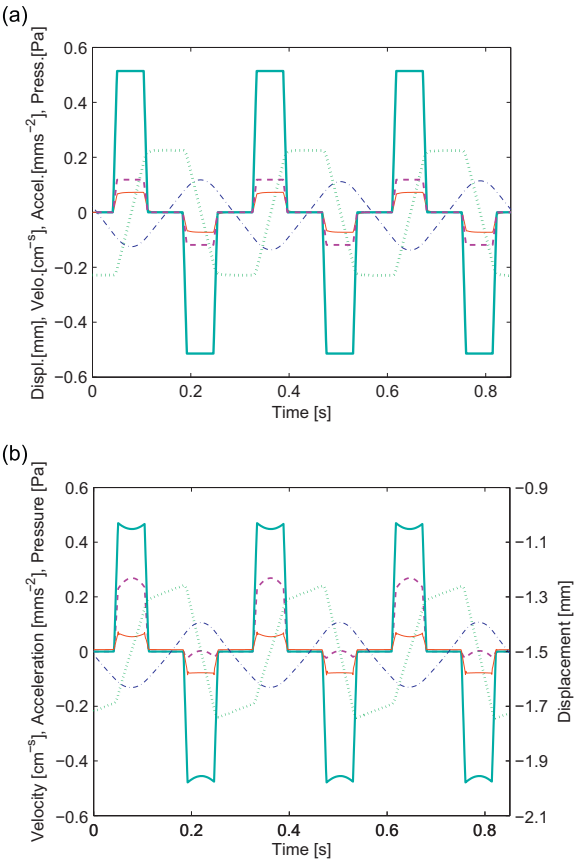

Fig. 8. Numerically predicted sound pressure and ball movements in horizontal direction, ——— pressure p_L, - - - - - - - - pressure p_R, ····· ball velocity, ——— ball acceleration, – · – · – · – · – · ball displacement. See Fig. 2 for the locations L and R close to the ball. (a) Steady state horizontal ball movement and pressure close to the ball, without large displacement effects. (b) Steady state horizontal ball movement and pressure close to the ball, including large displacement effects using a moving mesh.

in Fig. 2, a normal acceleration is specified as

$$-\mathbf{n}\cdot\left(-\frac{1}{\rho_0}\nabla p\right)=a_n, \tag{11}$$

where a_n is the acceleration of the moving body. A typical set-point that is used as a prescribed acceleration for the acoustic domain is given in Fig. 3. On the other boundaries of the moving body hard wall boundary conditions are specified:

$$-\mathbf{n}\cdot\left(-\frac{1}{\rho_0}\nabla p\right)=0. \tag{12}$$

The movement of the stage is enforced on the mesh, using the moving mesh approach as described in the paragraph "moving mesh".

As will be shown in Section 3.1, the measurement room is somewhat cluttered by different objects, this will cause reflection of the acoustic waves. It is therefore difficult to argue how to model the acoustic domain and what kind of boundary conditions holds best for the acoustic model. A mix of boundary conditions is used to approximate the actual situation as best as possible without resorting too much into modelling details. The acoustic domain consists of a rectangular room of $3\times3\times1.8$ m, as illustrated in Fig. 4. The bottom boundary of the acoustic domain, at a distance of 30 cm below the moving stage, is modelled as an acoustically rigid wall, representing the acoustical hard objects below the moving stage (see Fig. 12, Section 3.1). All other boundaries of the acoustic domain are modelled as non-reflecting, sound absorbing walls.

On the sound absorbing walls the radiation boundary condition is applied. It allows an outgoing wave to leave the modelling domain with no or minimal reflections. For transient analysis types the radiation condition is implemented in Comsol using Givoli and Neta's formulation of the Higdon condition [6] up to the first order. Unfortunately, such a formulation is exact only if the plane acoustic wave is incident on the artificial boundary at normal incidence angle. At an oblique incidence, significant reflection may occur, say, at the corners of the rectangular computational domain. Therefore, the radiation boundary condition used in the current paper is not an exact outgoing wave condition, and sound reflection exists due to the oblique incidence angle. However, in view of the approximate nature of the boundary conditions chosen,

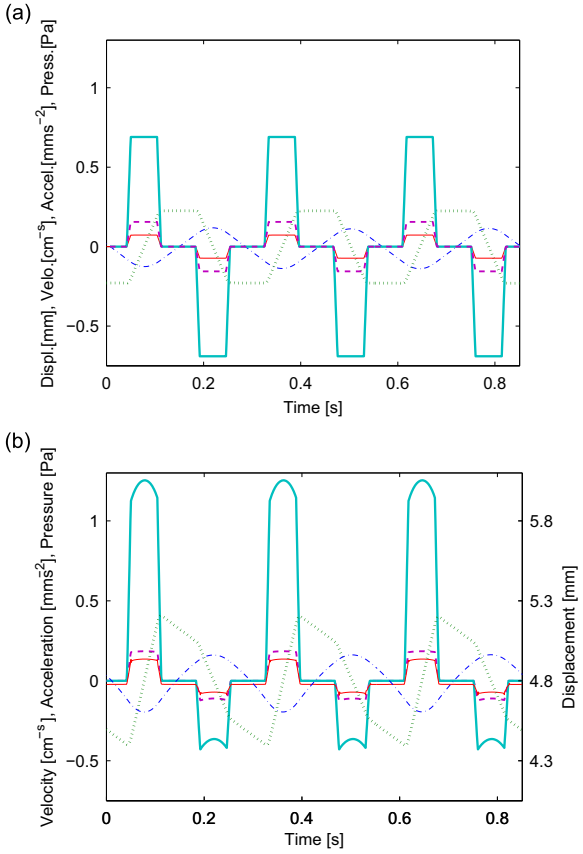

Fig. 9. Numerically predicted sound pressure and ball movements in vertical direction, ——— pressure p_T, - - - - - - - - pressure p_B, ····· ball velocity, ——— ball acceleration, — · — · — · — · — ball displacement. See Fig. 2 for the locations T and B close to the ball. (a) Steady state vertical ball movement and pressure close to the ball, without large displacement effects. (b) Steady state vertical ball movement and pressure close to the ball, including large displacement effects using a moving mesh.

as discussed in the previous paragraph, and because of the dominant reflection of the bottom boundary, this deficiency is considered to be acceptable for the current purpose.

2.1.6. Moving mesh

To allow for a large displacement, an arbitrary Lagrangian–Eulerian (ALE) technique is used to solve the coupled structural-acoustic problem in combination with a moving mesh approach. The spatial coordinates are denoted by (x,y) and (X,Y) are the coordinates of a mesh node in the initial, undeformed configuration. To describe the spatial coordinates (x,y) of the same mesh node in the deformed configuration, the following functions are used:

$$x = x(X,Y,Z,t), \quad y = y(X,Y,Z,t) \quad z = z(X,Y,Z,t), \tag{13}$$

where t is time. This coordinate transformation relates two frames (see Fig. 5), for simplicity shown in two dimensions:

- The spatial frame is the usual, fixed coordinate system with the spatial coordinates (x,y). In this coordinate system the mesh is moving, that is, the coordinates (x,y) of a mesh node are functions of time.
- The reference frame is the coordinate system defined by the reference coordinates (X,Y). In this coordinate system the mesh is fixed to its initial position. One can view the reference frame as a curvilinear coordinate system that follows the mesh.

A Winslow mesh smoothing algorithm is used to calculate the transformation from the reference coordinates (X,Y) to the deformed coordinates (x,y), such that the inverse transformation $X=X(x,y)$, $Y=Y(x,y)$ fulfils the Laplace equation:

$$\frac{\partial^2 X}{\partial x^2} + \frac{\partial^2 X}{\partial y^2} = 0, \quad \frac{\partial^2 Y}{\partial x^2} + \frac{\partial^2 Y}{\partial y^2} = 0, \tag{14}$$

over the whole domain [7–9]. In this manner the mesh is deformed smoothly, allowing a large displacement without collapsed or distorted elements. This moving mesh procedure can easily be generalized into three dimensions.

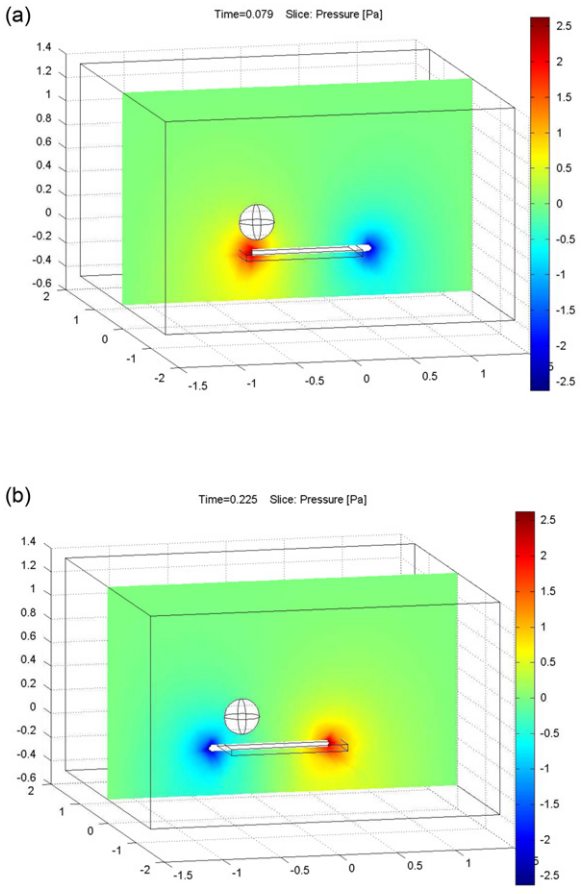

Fig. 10. Numerically predicted sound pressure field radiated by the stage at two extreme positions. (a) Time step at $0.278 \times 2\pi$ rad. (b) Time step at $0.792 \times 2\pi$ rad.

Fig. 6 gives an overview of the numerical modelling procedure, with the various physical domains, modelled in Comsol.

2.2. Numerical results

The three dimensional simulations were carried out for the stage set-point as shown in Fig. 3, applying the accelerations to the acoustic domain boundary conditions and enforcing the stage displacements on the mesh. During the simulations the sound pressure field around the moving stage and the ball is calculated, as well as the ball motions. The stage radiates acoustic noise during acceleration and deceleration only, as can be seen from Fig. 7. From literature [10] it is known that very close to a vibrating surface, the sound pressure is closely related to the local surface normal acceleration, the sound pressure being nearly in quadrature with the local particle velocity. This is also reflected in this case, in which the pressure in the acoustic domain is either positive, or negative, only during the acceleration and deceleration of the stage. During parts of the cycle with constant velocity of the stage, no acoustic noise is being generated.

In the FE model the ball is suspended with weak springs without damping. The only physical damping mechanisms included in the FE model is radiation damping. Due to the fact that the radiation damping of the ball is extremely low, it takes very long for the pendulum motion of the ball to achieve steady state. The simulation results that are shown in this paper, however, consider only steady state behaviour.

Below the geometric nonlinear effect on the ball motion is studied in more detail. Fig. 8(a) and (b) shows the steady state horizontal movements of the ball and the pressure p_L and p_R just to the left and right of the ball as function of time, using a linear simulation (not taking into account the large displacement effects) and a moving mesh simulation, respectively. Note that in Fig. 8(b) a different ordinate scale is used for the ball displacement. It is remarkable to see that at steady state the ball is displaced by about 1.5 mm to the left if the large displacement effects are taken into account. On top of this offset displacement the ball vibrates due to the acoustic pressure fields radiated by the oscillating stage. The offset displacement is caused by an asymmetry in the pressure field as function of time, which is most apparent for the pressure on the right of the ball, p_R, as can be seen from Fig. 8(b).

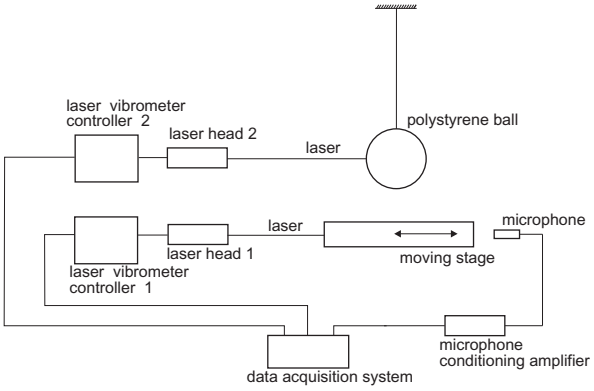

Fig. 11. Schematic overview of moving stage experimental setup.

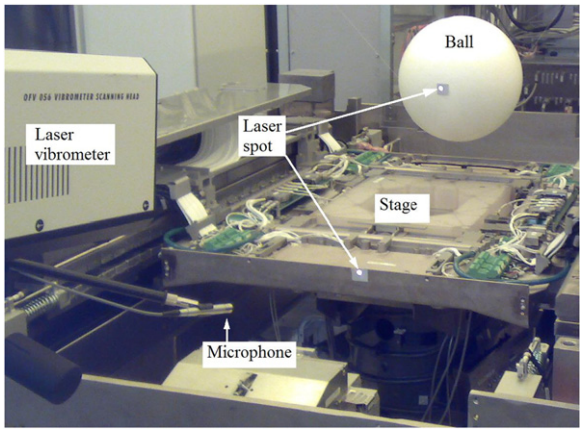

Fig. 12. Moving stage experimental setup, showing stage, polystyrene ball hanging on a thin rope, microphone, laser vibrometer (only one is shown), and arrows pointing at vibrometer laser spots.

Fig. 9(a) and (b) shows the steady state vertical movements of the ball and the pressure just at the top and bottom of the ball as function of time, again using a linear simulation and a moving mesh simulation, respectively. Note that in Fig. 9(b) a different ordinate scale is used for the ball displacement. In vertical direction the offset of the ball is even higher, amounting to an upwards movement of about 5.2 mm, taking the large displacement effects into account. The asymmetry in the pressure field as function of time, as measured at the bottom of the ball is indeed significant, causing offset displacement of the ball in vertical direction.

The asymmetry in the pressure field around the ball, which gives rise to harmonic distortion of the pressure signal, finds its cause in the large displacement of the stage. As concluded earlier, a vibrating structure radiates acoustic noise from the surfaces that have a positive or negative acceleration component in normal direction. In case of the stage these are the front and rear surfaces. Due to the large displacement of the stage, these surfaces are at rather different positions relative to the ball during acceleration and deceleration, respectively. This fact is illustrated by Fig. 10, in which the pressure

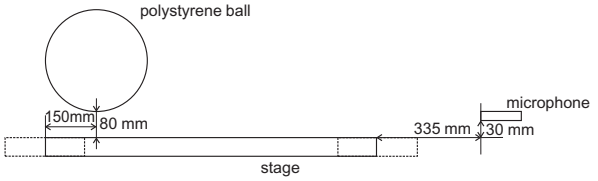

Fig. 13. Measurement positions of polystyrene ball and microphone, relative to the stage. Dimension polystyrene ball $R=150$ mm. The dashed line shows the outer left and outer right position of the stage.

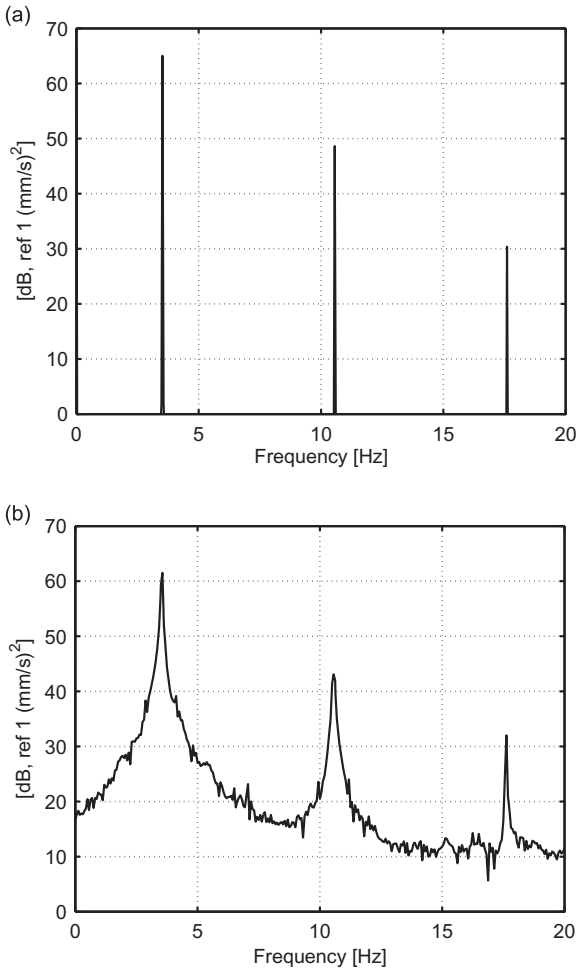

Fig. 14. Autospectra stage velocity. (a) Theoretical autospectrum stage velocity (set-point input). (b) Measured autospectrum stage velocity (single head laser).

distribution around the ball is given for two extreme positions of the stage. In Fig. 10(a) it can be seen that the positive pressure is generated directly beneath the ball, whereas its negative counterpart, half a period later in time (Fig. 10(b)) is generated relatively far away from the ball. This causes the positive sound pressure acting at the bottom of the ball to be much higher in magnitude than the magnitude of the negative sound pressure, as can be seen in Fig. 9(b) also. Note that such an asymmetric function of time can only be described by using both odd and even harmonics of the fundamental frequency, which implies the existence of harmonic distortion for input functions that contain odd harmonics only, as shown in Fig. 3. This fact will be treated in more detail in the next section.

As a consequence of the offset displacements in horizontal and vertical directions, the spring will exert a force on the ball in both directions, giving a constant small acceleration downwards and to the right. This constant small acceleration downwards and to the right also accounts for the fact that the velocity v_x and v_z of the ball in horizontal and vertical directions, respectively, is never constant, even not when the acoustic pressure is zero, as can be seen in Figs. 9(b) and 8(b).

3. Experiments

The FE model is validated by means of experiments on a stage of a lithographic machine. The acoustic pressure in the vicinity of the moving stage is measured as well as the movements of a polystyrene ball hanging on a wire in close proximity of the wafer stage. In the next section the measurement setup is explained in more detail.

3.1. Test setup

A polystyrene ball with a weight of $m=0.2674$ kg and radius $a=0.15$ m is attached to the ceiling by means of a thin rope. The polystyrene ball is positioned above the moving stage, close to the end of the stage, leaving a clearance of 80 mm between the ball and the upper surface of the stage (see Fig. 13). Note that in practice a rather important secondary structure like the lens is at very close distance to the moving stage, which makes a clearance of 80 mm very realistic.

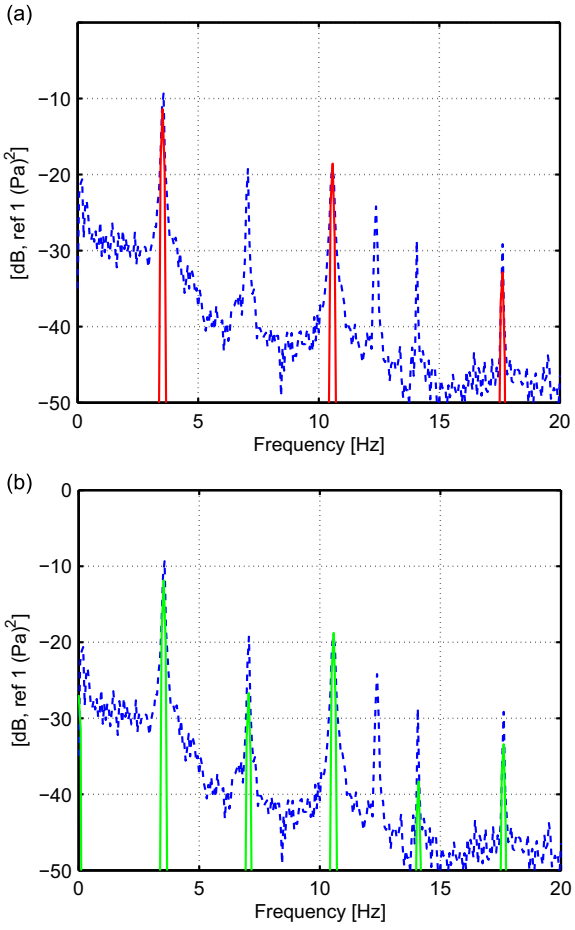

Fig. 15. Autospectrum sound pressure at microphone position, ———— simulation, - - - - - - - - experiment. (a) Linear small amplitude simulation and large amplitude experiment. (b) Nonlinear large amplitude simulation and large amplitude experiment.

A Brüel & Kjaer microphone type 4192 is placed in close proximity to the stage, at a distance of 335 mm from the edge of the stage in nominal position (see Fig. 13). Both the velocity of the polystyrene ball and the velocity of the stage are measured by means of laser vibrometers, a Polytec type OFV 303 and a Polytec type OFV 056. A schematic overview of the setup is given in Fig. 11. Fig. 12 shows a photograph of the test setup.

3.2. Stage movement settings

A typical scan set-point of a stage, as shown in Fig. 3, is used in the experiment. The total stroke (peak–peak displacement) of the stage is approximately 26 cm. The autospectrum of the synthesized velocity set-point is shown in Fig. 14(a). Contributions for the uneven harmonics are visible only, as expected because of the point symmetry of the set-point (see Fig. 3). The fundamental frequency of the set-point equals 3.52 Hz. The measured autospectrum of the velocity of the stage is shown in Fig. 14(b).

3.3. Experimental results and observations

The experimental and numerical data are considered in the frequency domain as autopower spectra. Fig. 15 presents the autospectra at the microphone position. Figs. 16 and 17 present the autospectra of the horizontal and vertical ball velocity, respectively. A number of observations can be made. The microphone measurements presented in Fig. 15 show that besides the contribution of the uneven harmonics of the set-point, the even harmonics are also visible because of the geometric nonlinear effect. The spectral component at 12.4 Hz is also noted without stage movement. Thus it can be concluded that this component is a background noise contribution which can safely be ignored for the present analysis. The autospectra of the velocity of the ball in horizontal direction, as shown in Fig. 16 also shows the presence of even harmonics, which are not present in the set-point. In vertical direction, where we can only rely on the numerical model because of the absence of experimental data, the same behaviour is found (Fig. 17).

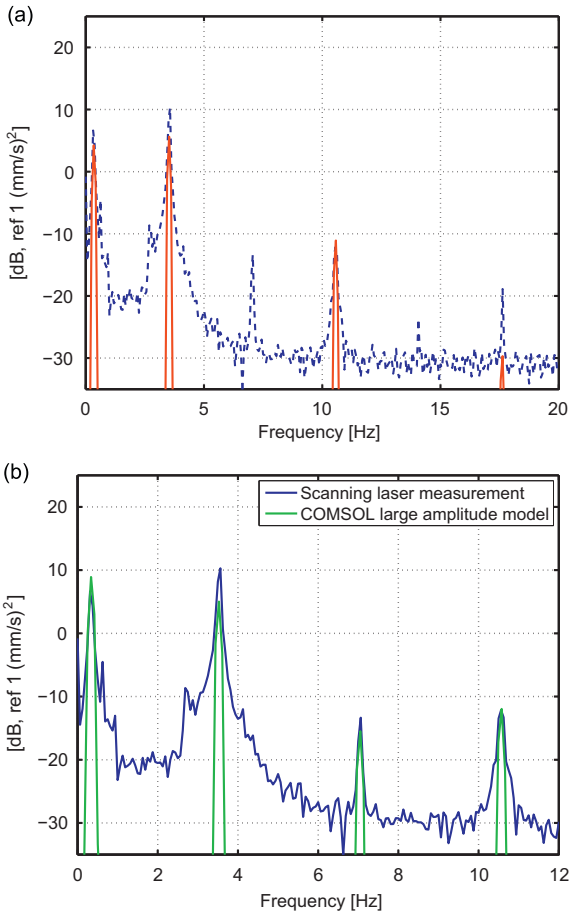

Fig. 16. Autospectrum horizontal ball velocity, ———— simulation, - - - - - - - - experiment. (a) Linear small amplitude simulation and large amplitude experiment. (b) Nonlinear large amplitude simulation and large amplitude experiment.

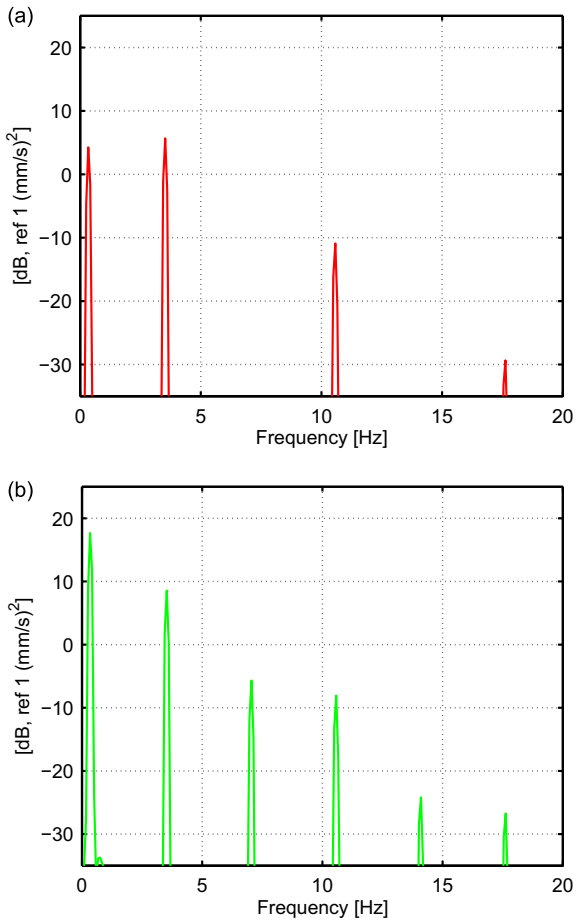

Fig. 17. Autospectrum vertical ball velocity, simulation. (a) Linear small amplitude simulation. (b) Nonlinear large amplitude simulation.

The presence of even harmonics, which are not present in the stage setpoint, is due to distortion effects. The distortion effects find its root cause in the asymmetry of the pressure signal as a function of time for a fixed observer, as discussed in the previous section. An asymmetric function of time, such as shown in Figs. 8(b) and 9(b), can only be described by using both odd and even harmonics of the fundamental frequency. Obviously, the linear model does not capture the asymmetry in the pressure signal and hence does not predict the harmonically distorted components such as the 2nd harmonic frequency component, nor in term of pressure (Fig. 15(a)), nor in terms of ball motion (Figs. 16(a) and 17(a)). The nonlinear model takes the geometric nonlinearity into account and does predict the harmonic distortion due to the time signal asymmetry, both in terms of pressure (Fig. 15(b)), and in terms of ball motion (Figs. 16(b) and 17(b)).

The strength of the large displacement induced harmonic distortion is significant. According to the measurements the strength of the sound pressure 2nd harmonic is 10 dB below the fundamental frequency, and about equal in strength as compared to the 3rd harmonic (Fig. 15). The 2nd harmonic component of the ball movement in horizontal direction is 23 dB below the fundamental component (20 dB according to the simulations). In vertical direction the harmonic distortion is more significant, being 15 dB below the fundamental component. In both the vertical and the horizontal directions the strength of the 2nd and 3rd harmonics are equally important, underlining the significance of harmonic distortion in this specific case.

For completeness, only one frequency contribution in the motion of the ball does not correspond to a harmonic frequency of the stage set-point, namely, the contribution at 0.343 Hz. Because the polystyrene ball is attached to the ceiling by a thin rope, it has a certain pendulum frequency, f_{pendulum}, which is determined by the length of the rope, l (m), and the gravitational constant, g (ms^{-2}). It is

$$T = 2\pi\sqrt{\frac{l}{g}} = 2\pi\sqrt{\frac{2.1}{9.81}} = 2.9\,\text{s}, \quad f_{\text{pendulum}} = \frac{1}{T} = 0.343\,\text{Hz}. \tag{15}$$

which is in close agreement with the measurements.

4. Conclusions

In this paper experiments and numerical analyses of the acoustic radiation from a lithographic moving stage are described. In the present study a finite element model is developed using a linear fluid behaviour in combination with a moving mesh approach to accommodate the large displacements. The model is successfully validated by experiments on a lithographic stage. It is shown that the geometric nonlinear effects lead to an asymmetry in the time signal of the radiated pressure as observed at a fixed position, which in turn causes harmonic distortion.

Having identified and modelled harmonic distortion by finite elements, it will be possible to include harmonic distortion in control loop design for lithographic stages to counteract the acoustically induced vibrations of the machine. This was not part of this study, but is expected to lead to a better control design.

Acknowledgements

The company ASML in Veldhoven, the Netherlands, and especially Dr. Hans Butler and Dr. Francois-Xavier Debiesme are acknowledged for their support and ideas. The authors thank the editor and reviewers for their constructive comments. The work was done while the second author was a student at the Dynamics and Control group, Department of Mechanical Engineering, Eindhoven University of Technology.

References

[1] P.M. Morse, K.U. Ingard, *Theoretical Acoustics*, McGraw-Hill, 1968.
[2] P.A. Frost, E.Y. Harper, Acoustic radiation from surfaces oscillating at large amplitude and small Mach number, *Journal of Acoustical Society of America* 58 (2) (1975) 318–325 10.1121/1.380675.
[3] T.L. Geers, K.S. Hunter, An integrated wave-effects model for an underwater explosion bubble, *Journal of Acoustical Society of America* 111 (4) (2002) 1584–1601 10.1121/1.1458590.
[4] N. De Jong, A. Bouakaz, P. Frinking, Basic acoustic properties of microbubbles, *Echocardiography* 19 (3) (2002) 229–240 10.1046/j.1540-8175.2002.00229.x.
[5] M.J. Crocker (Ed.), *Handbook of acoustics*, John Wiley & Sons, 1998 (Chapter 18).
[6] D. Givoli, B. Neta, High-order non-reflecting boundary scheme for time-dependent waves, *Journal of Computational Physics* 186 (2004) 24–46.
[7] A. Winslow, Numerical solution of the quasilinear Poisson equations in a nonuniform triangle mesh, *Journal of Computational Physics* 1 (2) (1966) 149–172 10.1016/0021-9991(66)90001-5.
[8] P.M. Knupp, Winslow Smoothing on two-dimensional unstructured meshes, *Engineering with Computers* 15 (3) (1999) 263–268.
[9] S.L. Karman, Mesh generation using unstructured computational meshes and elliptic partial differential equation smoothing, *AIAA Journal* 44 (6) (2006) 1277–1286.
[10] F.J. Fahy, *Foundations of Engineering Acoustics*, Academic Press, 2001 (Chapter 6.8).